IEEE Access
Multidisciplinary | Rapid Review | Open Access Journal

Received July 3, 2020, accepted July 26, 2020, date of publication July 30, 2020, date of current version August 13, 2020.

Digital Object Identifier 10.1109/ACCESS.2020.3013116

Design and Simulation of Thermo-Optic Phase Shifters With Low Thermal Crosstalk for Dense Photonic Integration

SOUVARAJ DE[1,2], (Student Member, IEEE), RANJAN DAS[1], (Member, IEEE), RAVI K. VARSHNEY[2], AND THOMAS SCHNEIDER[1]

[1]THz-Photonics Group, TU Braunschweig, 38106 Braunschweig, Germany
[2]Department of Physics, IIT Delhi, New Delhi 110016, India

Corresponding author: Ranjan Das (ranjan.das@ieee.org)

We acknowledge support by the Deutsche Forschungsgemeinschaft (DFG) through the Meteracom Project under Grant SCHN 614 507 10, Grant SCHN 614 507 11, Grant SCHN 614 507 12, Grant SCHN 614 507 13, and the Open Access Publication Funds of the Technische Universität Braunschweig.

ABSTRACT We investigate and demonstrate the thermal crosstalk problem in integrated photonic circuits with metal and silicon doped heaters. Further, we illustrate that due to the localized heating effect, integrated doped heaters are out-performed in terms of thermal crosstalk as compared to integrated metal heaters. To mitigate thermal crosstalk and enhance phase tuning efficiency further, a CMOS compatible air-filled trench region is realized between the doped heater and the adjacent element. The performances of three fundamental building blocks of integrated photonic circuits, namely, a PN phase shifter, an optical attenuator, and a ring resonator, are tested by full-wave thermal, charge, and optical simulations. Additionally, the impact of thermal crosstalk on the performance of integrated PN phase shifters and optical attenuators is examined thoroughly. The proposed low crosstalk thermal phase shifters might be very beneficial for densely routed complex integrated photonic circuits like photonic transceivers for data centers, optical phased array antennas, and photonic reservoirs.

INDEX TERMS Silicon on insulator (SOI), thermal crosstalk, phase shifter, integrated doped heaters, integrated optical attenuator, thermal switch, ring resonator.

I. INTRODUCTION

Compared to the electrical domain, signal processing in the optical domain, telecommunications, for instance, is a more viable option as it offers wide-bandwidth, relatively simple implementation, cost-effectiveness, power efficiency and provides strong immunity to electromagnetic interference (EMI). This can help to cope with the increasing global demands for high data rates to support new technologies and numerous modern applications like high-speed global networking, autonomous driving, the internet of things (IoT), etc. [1]. Consequently, there is a need for programmable processors and photonic signal processing based on integrated silicon photonics [2], since the existing electronic solutions are limited by power consumption and low bandwidth operation. In integrated photonics, a variety of optical functions namely modulation, multiplexing, wavelength filtering etc. can be integrated easily to create a full photonic system. Since silicon (Si) is transparent for the infrared wavelengths, it is commonly used in the telecommunications range. The most popular platform for integrated photonics is silicon-on-insulator (SOI) to leverage the well-established complementary metal oxide semiconductor (CMOS) technology [3], [4]. With silicon photonics, many diverse functionalities can be integrated on a single chip while the use of CMOS electronics adds control to the photonic elements.

As an important component of PICs, various thermo-optic phase shifters have been reported so far [5], [6] which were applied for many interesting applications including switching, sensing, advanced communication and neural networks in complicated devices like ring resonators, Mach-Zehnder interferometers (MZIs) and Mach-Zehnder modulator (MZM) arrays [7]–[9]. A thermo-optic phase shifter works by modulating the temperature of the waveguide with a resistive micro-heater, which induces a local modification of the refractive index and, in turn, a phase shift on

The associate editor coordinating the review of this manuscript and approving it for publication was Bora Onat.

the guided photons [10]. However, due to the inevitable thermal conductance of the chip material, the heating might lead to undesired crosstalk. This thermal crosstalk in integrated attenuators, commonly used to control the optical power in wavelength division multiplexed (WDM) networks [11]–[14] might lead to loss of confinement, reduced output power and eventually restrict its working capabilities. Similarly, PN phase shifters or ring resonator based thermal switching networks [15], [16] might lead to an erroneous signal routing due to thermal crosstalk.

To eliminate the undesirable changes due to the thermal crosstalk, an ultra-low loss thermo-optic phase shifter was reported in [17]. However, this design suffers from a large footprint and high-power consumption. In [18], a time-multiplexed row-column addressing scheme using a pulse width modulation (PWM) was proposed. Nevertheless, the scaling of this technique is limited by a maximum achievable phase shift, time constant, and other electrical design parameters. Three-dimensional trenches were used to reduce the thermal crosstalk while maintaining a smaller chip size [19]. However, such designs are customized and furthermore, the use of an external heat sink restricts its feasibility on the standard CMOS process. Additionally, special solutions like the Transform Coordinate Method (TCM) and Thermal Eigenmode Decomposition (TED) were presented in [20], [21], which shows promising results for microring resonators (MRR). A brief thermal crosstalk analysis for micro-disk resonators with heater-modulators was reported in [22]. Recently, thermal phase shifters based on doped heaters with improved performances were reported in [23]. However, the presented thermal crosstalk analysis was not comprehensive and some amount of the heat is dissipated through the silicon substrate limiting the efficiency.

To improve the heating efficiency and minimize the thermal crosstalk issue for integrated thermal phase shifters, we come up with a simple design modification. Instead of using conventional metal heaters, we consider doped silicon heaters placed close to the main waveguide to obtain the desired phase changes by a local heating effect. Additionally, the residual crosstalk can be removed further by providing thermal isolation from the doped heater by implementing air-filled trenches between the doped heater and the adjacent elements. Major contributions of this work include: (i) a performance comparison in terms of thermal efficiency and crosstalk between metal and doped silicon heaters on an SOI platform is examined and discussed, (ii) impact of thermal crosstalk on the performance of PN phase shifters and optical attenuators is investigated for the first time, (iii) the detailed analysis of the crosstalk mitigation and phase tuning efficiency enhancement by standard fabrication compatible air-filled trench region is presented comprehensively, (iv) finally, full-wave 3D simulation results are provided and discussed to verify the effectiveness of the proposed air-filled trenches on the performances of three basic photonic components: integrated optical attenuators, PN phase shifters, and ring resonators.

This article is organized as follows: Sec. II analyzes performances of integrated metal and doped silicon heaters and presents a partial optical switching network to compare the thermal crosstalk performances of both heaters. Sec. III discusses a doped heater with an air-filled trench to reduce thermal crosstalk substantially. The effect of thermal crosstalk for three basic integrated elements: PN phase shifters, optical attenuators, and ring resonators are verified by the full-wave thermal, charge, and optical simulations in Sec. IV followed by a conclusion in Sec. V.

II. INTEGRATED HEATERS

Being widely used to design thermal phase shifters within photonic integrated circuits, integrated heaters are important elements in silicon photonics. Practically, two types of integrated heater designs are possible in an SOI platform: a metal heater, just above the waveguide on top of the silicon dioxide (SiO_2) layer [24]–[26] and doped silicon strips in close proximity to one side of the waveguide [26], [27]. A detailed discussion about the integrated heaters was provided in [28]. In this work, both heaters will be examined to compare the relative performance in terms of thermal crosstalk.

The temperature dependent phase change in the heated waveguide depends on the thermo-optic coefficient of both core (silicon) and cladding (silica) and it can be expressed as [26]:

$$\Delta\phi = \frac{2\pi L \Delta T \frac{dn_{eff}}{dT}}{\lambda_0} \tag{1}$$

$$\frac{dn_{eff}}{dT} = \frac{dn_{eff}}{dn_{Si}}\frac{dn_{Si}}{dT} + \frac{dn_{eff}}{dn_{SiO_2}}\frac{dn_{SiO_2}}{dT} \tag{2}$$

where n_{eff} is the effective index of the mode, L is the heater length, λ_0 is the wavelength in free-space , $\frac{dn_{Si}}{dT}$ and $\frac{dn_{SiO_2}}{dT}$ are the thermo-optic coefficient for silicon ($\sim 1.8 \times 10^{-4}$ K^{-1}) and silicon dioxide ($\sim 1 \times 10^{-5}$ K^{-1}), respectively, at $\lambda_0 =$ 1550 nm and $T = 300$ K, and ΔT is the temperature change, which for a π phase shift is computed as:

$$\Delta T\,(\pi) = \frac{\lambda_0}{2L\frac{dn_{eff}}{dT}} \tag{3}$$

As can be seen from (3), increasing L reduces $\Delta T(\pi)$, which eventually reduces lateral crosstalk. However, the device footprint and the propagation loss also increases for longer heaters. Therefore, the length of the heater is designed to be small. Additionally, to improve the thermal efficiency of the heater, the heat source is placed as close as possible to the waveguide. However, there must be some gap between the integrated heater and the waveguide to avoid metal-induced optical loss [25].

A. PERFORMANCE COMPARISON OF INTEGRATED HEATERS

In our simulations, the buried oxide (BOX) thickness is 2 μm and silicon dioxide (SiO_2) is the material used for the BOX and cladding layer. In every case, the thickness and width of

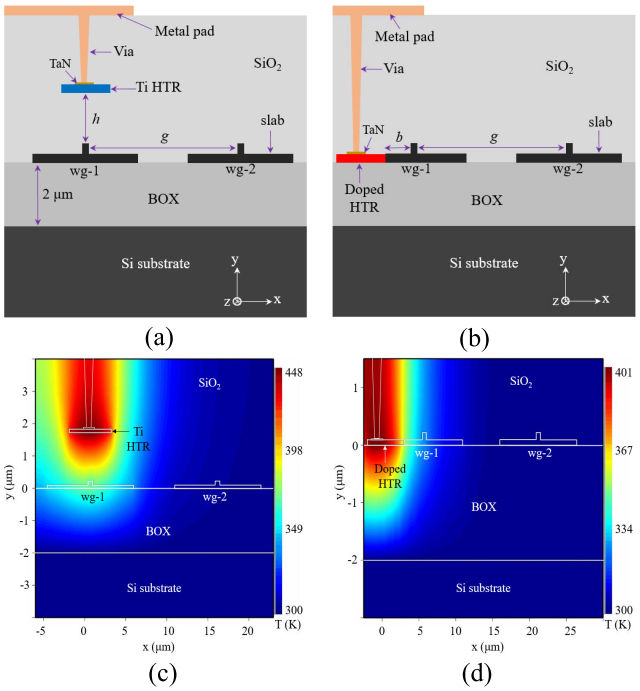

FIGURE 1. Geometry of silicon rib waveguides with: (a) titanium heater (Ti HTR), (b) N^{++} doped-silicon heater (Doped HTR), and the temperature profiles (different scale) for the (c) Ti heater, and (d) doped heater with heater power = 150 mW, gap (g) = 15 μm.

the rib waveguides are 220 nm and 500 nm to support a single TE-like mode at $\lambda_0 = 1550$ nm. The cross-sections of the titanium (Ti) based and the N^{++} doped silicon heaters are simulated by combining the thermal solver and the optical solver in Lumerical [29], to compare the heat distributions and the phase crosstalk, or an unintended phase change to the adjacent waveguide (wg-2 in Fig. 1(a) and (b)). The metal heater is made of titanium and is located at a height (h) of 1.5 μm above the rib waveguides with the thickness and width of 0.1 μm and 5 μm, respectively as shown in Fig. 1(a). The doped heater material is N^{++} doped silicon with a doping concentration of 1×10^{20} cm^{-3} and located along the rib waveguides as depicted in Fig. 1(b), with a heater thickness of 0.09 μm and a width of 5 μm. In both cases, the silicon slab has a thickness and width (w) of 0.09 μm and 10.5 μm, respectively. The gap g between the waveguides is varied from 2 μm to 15 μm to calculate the thermal crosstalk between the waveguides in each case. In addition, for the doped heater, there is a separation distance (b) of 2.5 μm between the doped heater and the waveguide (wg-1 in Fig. 1(b)) to prevent free-carrier absorption. The doped heater can be placed closer to the main waveguide to improve thermal efficiency. However, it will also increase the thermal crosstalk and metal-induced optical loss [25]. It might be beneficial in some applications where thermal efficiency is a major concern and some amount of crosstalk is affordable.

The ambient temperature for the thermal simulation is considered as 300 K and fixed convection of 10 W/m^2·K [29] is considered between the oxide layer and the air above it. The thermal and optical simulations of titanium and N^{++} doped silicon heaters with aluminum (Al) contacts are carried out using the finite element method (FEM) and finite- difference time-domain (FDTD) solvers respectively in Lumerical software [29]. Thereafter, the temperature profiles are imported to the optical solver, where the phase shifts are determined for a waveguide length of 300 μm.

Both heaters cause a temperature rise in the main waveguide (wg-1, where it is desired) and the adjacent waveguide (wg-2, where it is crosstalk), which changes the refractive index and therefore the phase shifts in the respective waveguides. However, the phase change in the main waveguide (wg-1) is desirable whereas it causes thermal crosstalk for the second waveguide (wg-2) and hence leads to undesired phase change or phase crosstalk. The temperature profiles for rib waveguides with different types of heaters are presented in Fig. 1(c) and (d). For the same amount of heater power, the titanium (Ti) heater reaches a much higher temperature as compared to the N^{++} doped silicon heater. In other words, metal heaters are thermally more efficient than doped heaters. A similar conclusion was reported earlier in [26]. The simulated thermal efficiencies (calculated as power required for a phase shift of π) of the titanium and doped silicon heaters are 34.4 mW and 45.1 mW, respectively. With metal (Al) contacts, the power consumption increases by 40% in both Ti and N^{++} doped silicon heaters. This is because some amount of power is dissipated through the metal contacts and it also acts as a heat absorber, which further reduces the heater temperature. However, the design of the metal contacts can be optimized to reduce power consumption as described in [26].

The phase crosstalk ratio, defined as the ratio of the phase shift in the second waveguide (wg-2) to the phase shift in the main one (wg-1), is calculated for both heaters and depicted in Fig. 2. Note that, the phase crosstalk is much lower for the doped heater, especially for smaller waveguide gaps (g). This is a result of the localized heating by a doped heater, whereas, for the metal heater, the entire region including the second waveguide is heated inadvertently. Therefore, doped heaters are preferred in applications where thermal crosstalk is of paramount importance and the additional heater power consumption is affordable. Later on, we will demonstrate power efficient thermal phase shifters based on doped-silicon heater in Sec. III. However, in most applications, it is required to design the photonic circuits exhibiting low thermal crosstalk for the proper functioning of the integrated network which will be explained with an example in the next subsection.

B. PARTIAL THERMAL SWITCHING NETWORK

To better illustrate the thermal crosstalk problem, a part of the ring resonators based switching network [15] is simulated with a Ti and an N^{++} doped Si heater. The Ti heater (inner radius $r_i = 9.275$ μm, thickness $d = 1$ μm and width $w = 0.3$ μm) is placed at a height of 1.5 μm directly above the ring ($r_i = 9.5$ μm, $d = 220$ nm, $w = 0.5$ μm, outer radius $r_o = 10$ μm), as shown in Fig. 3(a). Similarly, the N^{++} doped Si heater ($r_i = 4.55$ μm, $d = 3$ μm, $r_o = 7.55$ μm) is located

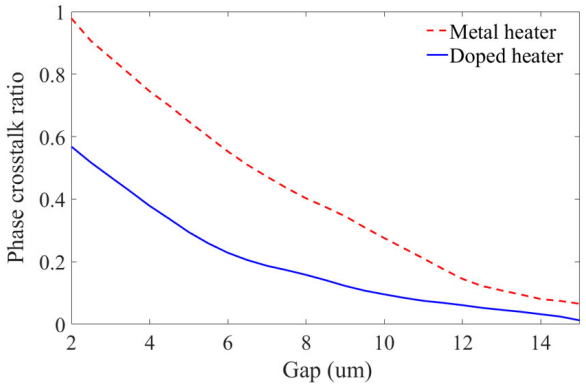

FIGURE 2. Phase crosstalk ratio in the second waveguide (wg-2 in Fig. 1) for metal and doped-silicon heaters (waveguide length = 300 μm).

in the same plane as the ring waveguide with a gap of 2 μm in the form of a ring, which separates the doped heater and the ring waveguide as shown in Fig. 3(b).

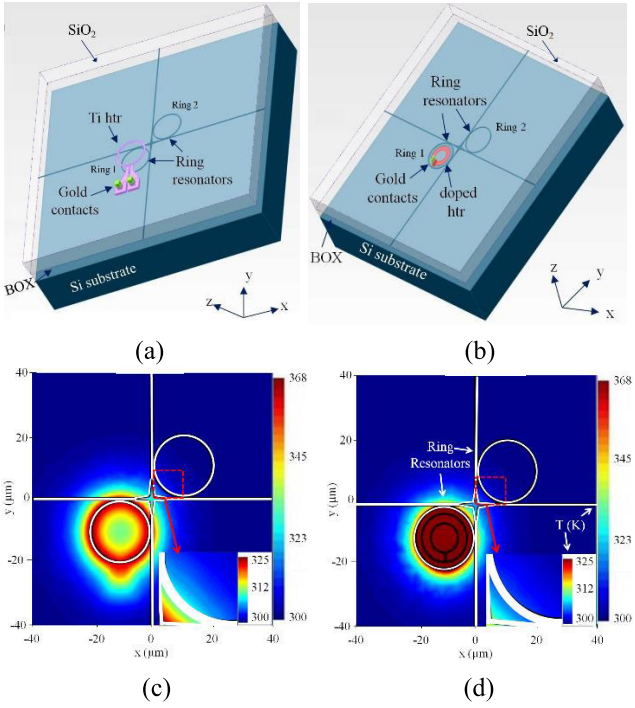

FIGURE 3. 3D geometry of the partial thermal switching network consisting of two ring resonators with: (a) Ti heater and (b) N^{++} doped silicon heater. The temperature profiles of the ring resonators with: (c) Ti heater and (d) N^{++} doped silicon heaters; the insets show the heating effect on a segment of the second ring resonator.

For both cases, the first ring (Ring 1) is heated up to a temperature of 368 K, as illustrated in Fig. 3(c) and (d). Due to the crosstalk between the rings, the directly adjacent part of the second ring resonator is heated up to 312 K in the case of Ti heater and 303 K for N^{++} doped silicon heater. Therefore, the spurious resonance frequency shift in the second ring (Ring 2) due to the crosstalk is higher for the Ti heater than for the doped-silicon heater, which might lead to an erroneous signal routing in the network.

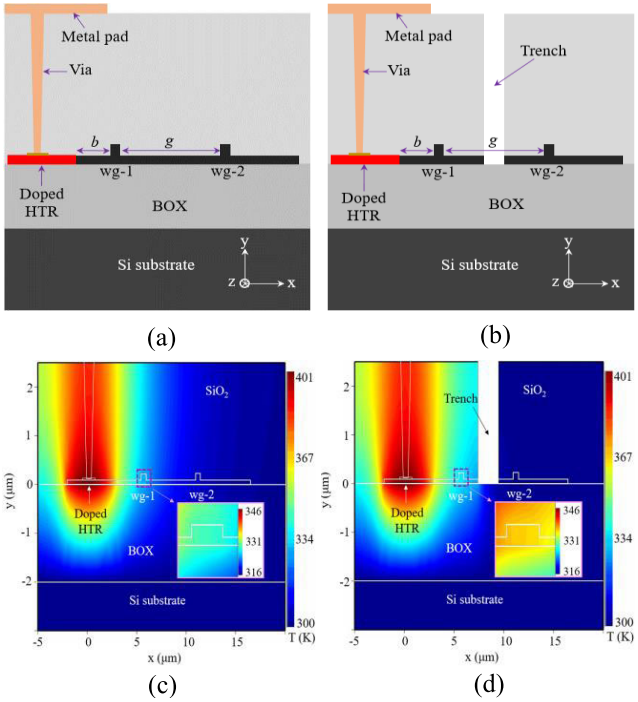

FIGURE 4. Rib waveguides for an N^{++} doped silicon heater with metal contacts: (a) without trench and (b) with an air-filled trench, and (c)-(d) Corresponding temperature profiles for a gap (g) of 5 μm and a heater power of 150 mW. Insets show a zoomed view of temperatures at the main waveguide (wg-1).

III. DOPED INTEGRATED HEATER WITH AIR-FILLED TRENCH

As discussed, due to the localized heating, doped heaters initiate less thermal crosstalk. However, the thermal crosstalk can be further mitigated by implementing an air-filled trench region between the rib waveguides, as shown in Fig. 4 (b). It starts from the BOX layer and extends up to top layer, while covering a region of around 70% along the waveguide length. The trench is placed at a gap of 2 μm from the waveguide core which supports the standard fabrication process. However, it can be placed closer to the waveguide to improve thermal efficiency. Also, such air-filled trench regions can be implemented by oxide etching (cladding removal) or by etching of both oxide and silicon to form the deep trenches.

The trench effectively provides thermal shielding to the adjacent integrated elements as air has a very low thermal conductivity of 0.026 W/m·K. To verify the effectiveness of the air-trench, full-wave thermal and optical simulations have been performed on rib waveguides, as depicted in Fig. 4(c) and (d). For the air-filled trench, the thermal crosstalk is very low and the adjacent waveguide remains almost at the ambient temperature of 300 K as demonstrated in Fig. 4(d). To estimate the undesired phase change in the second waveguide, the phase crosstalk ratio (the ratio of phase shift in the second waveguide to the phase shift in the main waveguide) for both scenarios is shown in Fig. 5(a). Note that, the phase crosstalk is reduced by around six times for a gap (g) of 5 μm and improves further with decreased gap

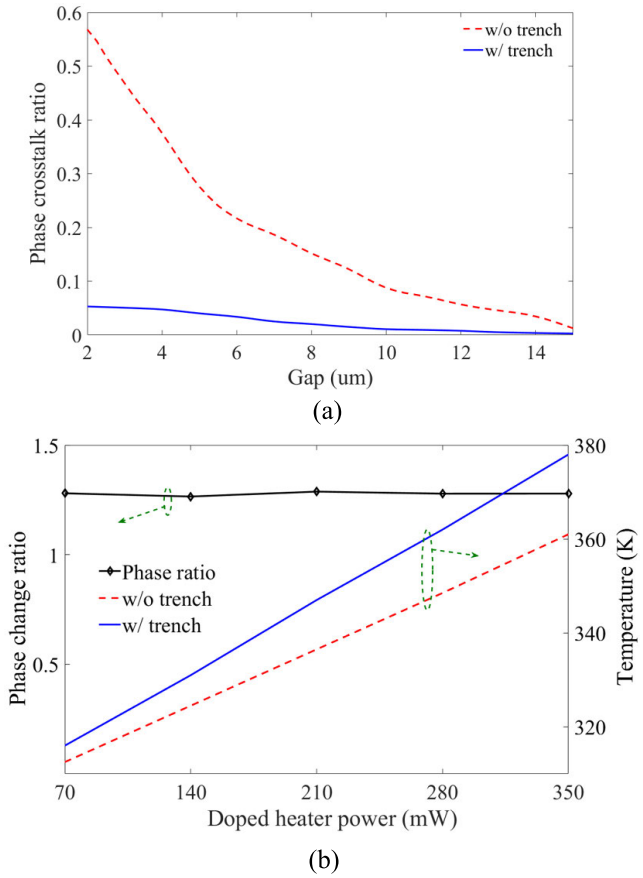

FIGURE 5. (a) Comparison of phase crosstalk ratio between without and with air-filled trench cases and (b) phase change ratio and temperature plot of the main waveguide (wg-1 in Fig. 4) for a length of 500 μm.

size. Furthermore, the air-filled trench region also helps to localize the heating effect within the main waveguide (wg-1) as demonstrated in the insets of Fig. 4(c) and (d). Thus, the same amount of phase shift can be obtained for a much lower heater power while maintaining the thermal crosstalk at a low level. To quantify the phase shift or thermal efficiency improvement, the phase change ratio, defined as the ratio of phase shifts in the main waveguide (wg-1) for with and without trench scenarios, is simulated (for a waveguide length of 500 μm) and plotted in Fig. 5(b). It is clear that the phase shift is improved by 30% if the trench is present. In other words, the power consumption is reduced by the same amount which compensates the additional power requirement of the doped heater as compared to the metal heater as mentioned in Sec. II.

IV. APPLICATION EXAMPLES

To illustrate and validate the thermal crosstalk performance of the proposed air-filled trench in conjunction with an embedded N^{++} doped silicon heater, three basic photonic components, namely, a PN phase shifter, an integrated optical attenuator, and a ring resonator are analyzed. All three components are placed in the vicinity of a thermally tuned waveguide for the crosstalk analysis.

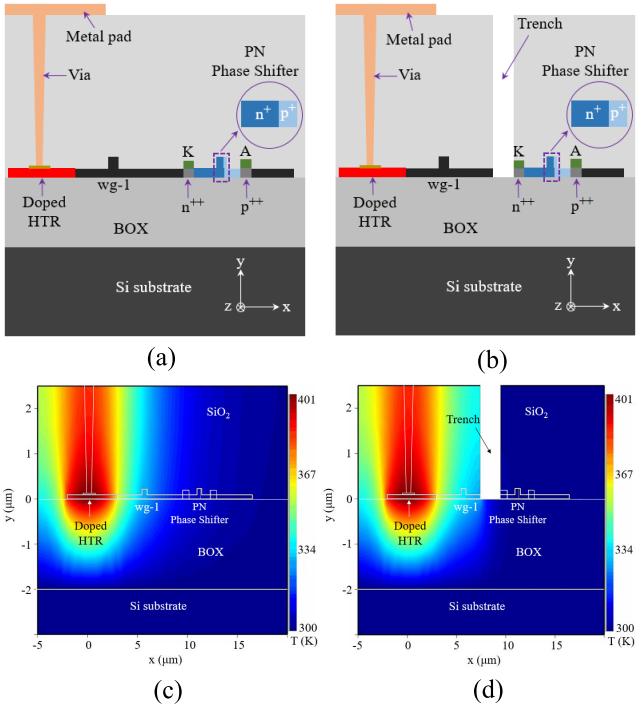

FIGURE 6. Cross-section views of a thermally tuned waveguide (wg-1) and a PN phase shifter: (a) without trench and (b) with a trench. Temperature profiles with a gap of 5 μm and a heater power of 150 mW for (c) no trench and (d) with an air-filled trench.

A. EXAMPLE I: INTEGRATED PN PHASE SHIFTER

To estimate the phase change due to the thermal crosstalk effect, a PN phase shifter [30] is placed at a distance of 5 μm from a thermally tuned waveguide (Fig. 6(a) and (b)). The air-trench region is implemented at the center of the gap. The PN phase shifter is operated at reverse bias using aluminum (Al) electrodes (A and K) with a doping concentration of 1×10^{20} cm^{-3} for the n^{++} and p^{++} wells, 4×10^{17} cm^{-3} for the n^{+} well, and 2×10^{17} cm^{-3} for the p^{+} well [29]. As can be seen from the temperature profiles in Fig. 6(c) and (d), the air-trench acts as a thermal barrier, and hence the PN phase shifter experiences lesser heating. Thereby, the sharp phase rise in the PN phase shifter with increased doped heater power is mitigated, as depicted in Fig. 7. For instance, at a doped heater power of 350 mW, the normalized phase at PN phase shifter is reduced by a factor of around ten and hence a significant reduction in thermal crosstalk. Therefore, the air-filled trench effectively isolates the PN phase shifter from the high temperature doped heater.

B. EXAMPLE II: INTEGRATED OPTICAL ATTENUATOR

The second example is an integrated optical attenuator [31], analyzed with and without trench, as shown in Fig. 8(a) and (b), respectively. It is placed at a gap of 5 μm from the thermally tuned main waveguide. The attenuator consists of p^{+}-i-n^{+} junctions and it is biased to operate in the carrier injection mode (forward bias). The aluminum electrodes (A and K) are used to apply a forward bias voltage

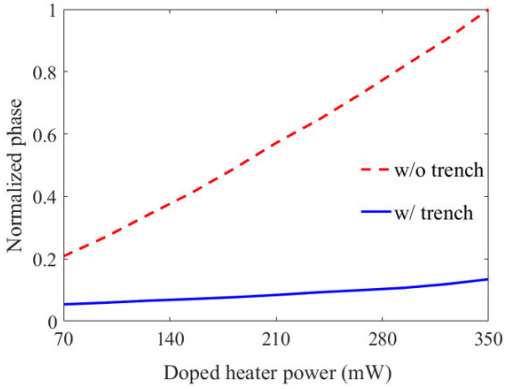

FIGURE 7. Comparison of the normalized phase for the trench and no trench case (Fig. 6) at zero bias voltage. The phase shift at PN phase shifter is normalized by the phase shift of the thermally tuned waveguide (wg-1) for a doped heater power of 350 mW.

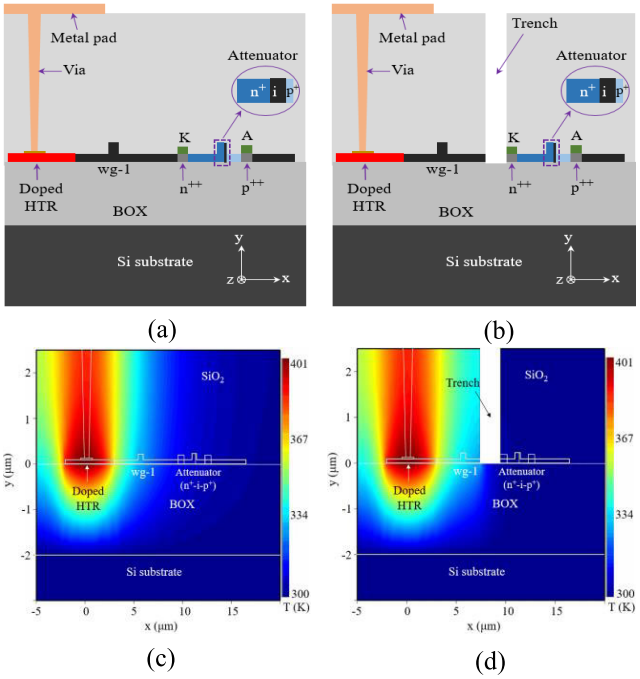

FIGURE 8. Cross-section of an integrated optical attenuator with (a) no trench and (b) an air-filled trench. Temperature distributions for a heater power of 150 mW for (c) without trench and (d) with an air-filled trench.

of 0.8 V to the attenuator. The doping concentrations are: $1 \times 10^{20}\text{cm}^{-3}$ for the n^{++} and p^{++} wells, $4 \times 10^{17}\text{cm}^{-3}$ for the n^{+} well and $2 \times 10^{17}\ \text{cm}^{-3}$ for the p^{+} well [29]. The doped heaters are designed with the same dimensions as described in Fig. 1(b).

The air-filled trench is located at the center of the gap between the thermally tuned waveguide and the attenuator. It is evident from the temperature profiles in Fig. 8(c) and (d) that the attenuator is exposed to more thermal stress in absence of the air-trench region. The carriers from the p^{+} and n^{+} region diffuse into the intrinsic (i) region because the diffusion coefficient of holes and electrons depends on the temperature according to the following relation [32]:

$$\frac{D_{n,p}}{\mu_{n,p}} = \frac{kT}{q} \tag{4}$$

where D is the diffusion coefficient of the carrier, μ the carrier mobility, k is the Boltzmann constant, T is the temperature and q the electron charge and the subscripts n and p refer to electrons and holes, respectively.

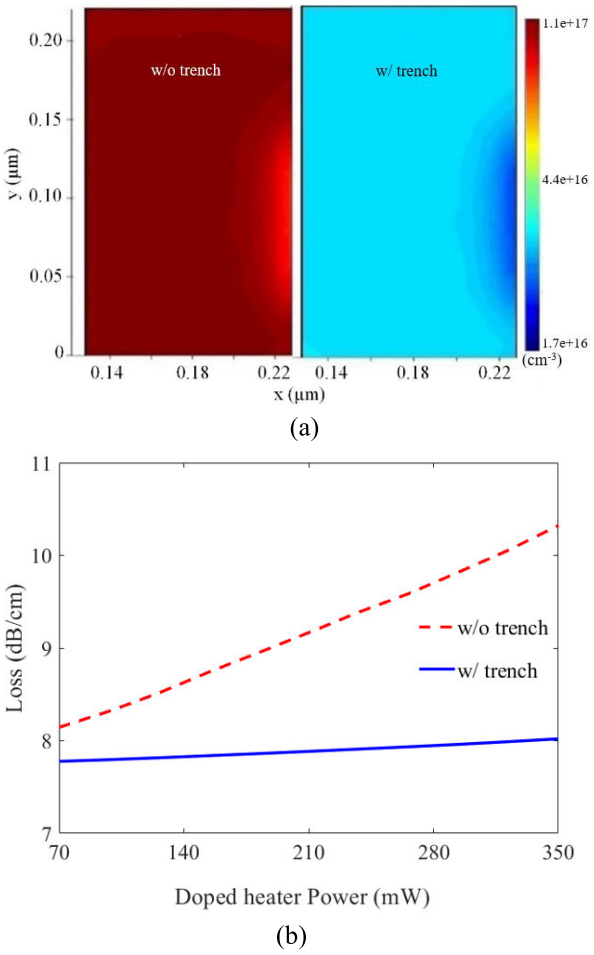

FIGURE 9. (a) Charge profile (in cm^{-3}) inside the intrinsic (i) region of the p^{+}-i-n^{+} attenuator without and with an air-trench for a heater power of 150 mW and (b) attenuator loss variation with power applied to the doped heater.

Consequently, at elevated heater temperature, a substantial amount of charge is diffused into the intrinsic (i) region of the p^{+}-i-n^{+} attenuator, which contributes to higher optical losses and degrades the attenuator performance. The charge distribution for both cases inside the intrinsic (i) region of the attenuator for a heater power of 150 mW is shown in Fig. 9(a) which reveals around eight times lesser charge concentration for the air-trench case. Therefore, the integrated optical attenuators become less susceptible to thermal crosstalk in presence of air-filled trench as demonstrated in Fig. 9(b). Moreover, for densely routed photonic circuits consisting of many thermal phase shifters, the attenuation increases further inadvertently due to the thermal crosstalk effect from adjacent phase shifters. To deal with this problem, the proposed air-trench provides a decent solution in which the attenuator loss remains almost constant for a fixed forward bias voltage

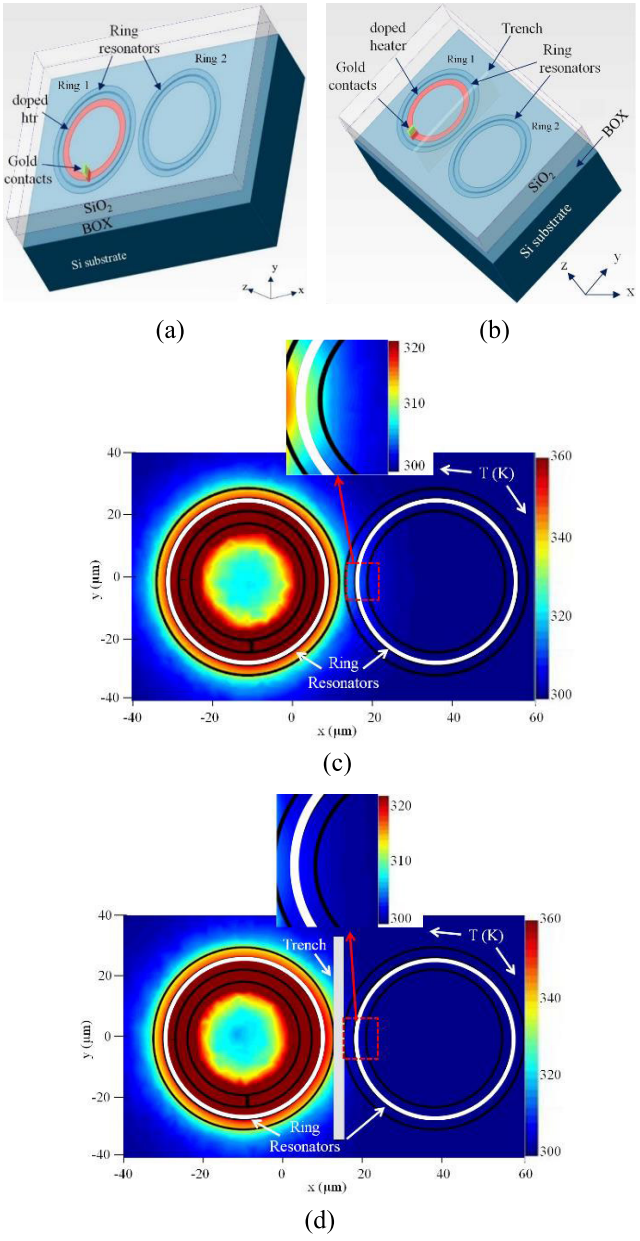

FIGURE 10. 3D geometry of two adjacent ring resonators (with an outer radius of 20 μm) and the heater (a) without trench, (b) with air-trench, and (c)-(d) corresponding temperature distributions.

and irrespective of powers at the adjacent doped silicon heaters.

C. EXAMPLE III: RING RESONATORS

Optical ring resonators, an important building block used as modulators, filters, or comb sources in photonic circuits, is examined finally for thermal crosstalk performance comparison. Two ring resonators are placed at a distance of 47 μm from their respective centers with a gap of 7 μm between the ring waveguides as shown in Fig 10. The N^{++} doped Si heater (inner radius $r_i = 14$ μm, outer radius $r_o = 17$ μm, thickness $d = 0.09$ μm, and width $w = 3$ μm) is located in the same plane as the ring (Ring 1) waveguide. A silicon slab

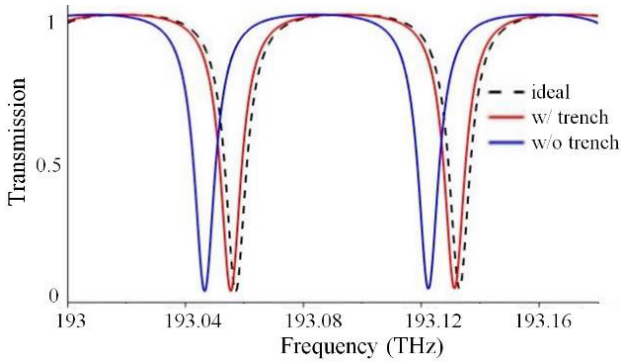

FIGURE 11. Optical transmission of the second (adjacent) ring resonator (with an outer radius of 166.5 μm) for different thermal crosstalk scenarios.

region of 2.5 μm thickness in the form of a ring separates the doped heater and the silicon waveguide (of Ring 1) as shown in Fig. 10(a) and (b). The rings are designed with a free spectral range (FSR) of around 625 GHz at $\lambda_0 = 1550$ nm with an outer radius of 20 μm. Also, there is a silicon slab region that extends on both sides of the ring waveguide with a width of 2.5 μm and a thickness of 0.09 μm to form the rib waveguide structure. Figure 10(b) has the same design as Fig. 10(a) except for an additional air-filled trench region that starts from the BOX layer and is placed equidistant from the centers of the ring resonators. Note that, in both scenarios (without and with trench), the resonance frequency shift of the adjacent ring (Ring 2) will be investigated to analyze the thermal crosstalk performance.

The thermal simulations are performed using the 3D thermal solver and subsequently, temperature profiles are imported to the optical solver [29] to determine the frequency shift of the ring resonators. As can be seen from the temperature distributions in Fig. 10(c) and (d), for the same amount of heating (around 360 K) in the first ring waveguide, the second ring waveguide is heated up to 312 K without and 302 K with an air-filled trench region, respectively. Due to a small rise in temperature, a minute resonance frequency drift is observed for the air-trench case.

To get an estimation of the resonance frequency shift, a different ring resonator with a free spectral range (FSR) of 75 GHz at $\lambda_0 = 1550$ nm (with an outer diameter of 166.5 μm) is verified, as depicted in Fig. 11. In the case of the doped heater without air-trench, the observed frequency shift is 11 GHz, which is almost 15% of the FSR. In contrast, the frequency shift is reduced to only 2% of the FSR for the air-filled trench scenario. Hence, the resonance frequency of the second ring is well-preserved by introducing an air-filled trench between the ring resonators.

In summary, the thermal crosstalk remains at a low level for all the three illustrative examples when an additional air-filled trench region is realized.

V. CONCLUSION

In this article, it has been shown through different full-wave simulations that a doped Si heater has better performance

than a conventional metal heater in terms of thermal crosstalk while the latter is more power-efficient. A part of an optical switching network has been verified to compare the thermal crosstalk performance for both types of heaters. Further, adding an air-filled trench region reduces the thermal crosstalk drastically and improves the phase shifter efficiency simultaneously. Three basic integrated photonic components, a PN phase shifter, an integrated optical attenuator, and a ring resonator have been verified through full-wave thermal and optical simulations. In the case of an optical attenuator, the attenuation factor remains unaffected due to the low thermal crosstalk. Similarly, the phase crosstalk and ring resonance shift, due to unwanted heating from adjacent integrated heaters, have been minimized significantly by the air-filled trenches. Due to its superior thermal crosstalk performance by a simple CMOS compatible design modification, the proposed doped heater based thermo-optic phase shifter with air-trenches is ideal for densely routed integrated silicon photonics circuits.

REFERENCES

[1] *Cisco Visual Networking Index: Forecast and Trends, 2017–2022*, White Paper c11-741490, Feb. 2019.

[2] D. Marpaung, J. Yao, and J. Capmany, "Integrated microwave photonics," *Nature Photon.*, vol. 13, no. 2, pp. 80–90, Feb. 2019.

[3] S. Gudyriev, C. Kress, H. Zwickel, J. N. Kemal, S. Lischke, L. Zimmermann, C. Koos, and J. C. Scheytt, "Coherent ePIC receiver for 64 GBaud QPSK in 0.25 μm photonic BiCMOS technology," *J. Lightw. Technol.*, vol. 37, no. 1, pp. 103–109, Jan. 1, 2019.

[4] L. Tsybeskov, D. J. Lockwood, and M. Ichikawa, "Silicon photonics: CMOS going optical [Scanning the Issue]," *Proc. IEEE*, vol. 97, no. 7, pp. 1161–1165, Jul. 2009.

[5] P. Dong, W. Qian, H. Liang, R. Shafiiha, D. Feng, G. Li, J. E. Cunningham, A. V. Krishnamoorthy, and M. Asghari, "Thermally tunable silicon racetrack resonators with ultralow tuning power," *Opt. Express*, vol. 18, no. 19, p. 20298, 2010.

[6] B. J. Offrein, D. Jubin, T. Koster, T. Brunschwiler, F. Horst, D. Wiesmann, I. Meijer, M. S. Petit, D. Webb, R. Germann, and G. L. Bona, "Polarization-independent thermooptic phase shifters in silicon-oxynitride waveguides," *IEEE Photon. Technol. Lett.*, vol. 16, no. 6, pp. 1483–1485, Jun. 2004.

[7] G. Coppola, "Advance in thermo-optical switches: Principles, materials, design, and device structure," *Opt. Eng.*, vol. 50, no. 7, Jul. 2011, Art. no. 071112.

[8] M. Jazayerifar, M. Namdari, R. Hamerly, D. Gray, C. Rogers, and K. Jamshidi, "Feasibility study of optical parametric amplification using CMOS compatible ring resonators," *Proc. SPIE*, vol. 10106, Feb. 2017, Art. no. 101060A.

[9] H. Hettrich and M. Möller, "A 5×11.3 Gbit/s MZM driver array with a 6 V_{pp} output voltage swing and a chip-to-chip bondwire interface in SiGe bipolar technology," in *Proc. IEEE Bipolar/BiCMOS Circuits and Technol. Meeting (BCTM)*, Boston, MA, USA, Oct. 2015, pp. 1–4.

[10] G. Cocorullo and I. Rendina, "Thermo-optical modulation at 1.5 μm in silicon etalon," in *Electron. Lett.*, vol. 28, no. 1, pp. 83–85, Jan. 1992.

[11] D. Agrawal and S. Bhattacharya, "Design and realisation of a MEMS based variable optical attenuator," in *Proc. Int. Workshop Phys. Semiconductor Devices*, Dec. 2007, pp. 695–698.

[12] A. Llobera, G. Villanueva, V. J. Cadarso, S. Battgenbach, and J. A. Plaza, "Polymeric MOEMS variable optical attenuator," *IEEE Photon. Technol. Lett.*, vol. 18, no. 22, pp. 2425–2427, Nov. 15, 2006.

[13] X. Ke, M. R. Wang, and D. Li, "All-optical controlled variable optical attenuator using photochromic sol gel material," *IEEE Photon. Technol. Lett.*, vol. 18, no. 9, pp. 1025–1027, May 1, 2006.

[14] E. Nicolescu, C. Mao, A. Fardad, and M. Escuti, "Polarization-insensitive variable optical attenuator and wavelength blocker using liquid crystal polarization gratings," *J. Lightw. Technol.*, pp. 3121–3127, Nov. 1, 2010.

[15] L. Zuxiang, L. Zhou, L. Lu, and J. Chen, "4×4 strictly non-blocking optical switch fabric based on cascaded multimode interferometers," in *Proc. 14th Int. Conf. Opt. Commun. Netw. (ICOCN)*, Jul. 2015, pp. 1–3.

[16] R. W. Chuang and M.-T. Hsu, "Dense multi-channel optical waveguide switch based on micro ring resonators," *J. Lightw. Technol.*, vol. 32, no. 8, pp. 1570–1577, Apr. 15, 2014.

[17] N. C. Harris, Y. Ma, J. Mower, T. Baehr-Jones, D. Englund, M. Hochberg, and C. Galland, "Efficient, compact and low loss thermo-optic phase shifter in silicon," *Opt. Express*, vol. 22, no. 9, pp. 10487–10493, May 2014.

[18] A. Ribeiro, S. Declercq, U. Khan, M. Wang, L. V. Iseghem, and W. Bogaerts, "Column-row addressing of thermo-optic phase shifters for controlling large silicon photonic circuits," *IEEE J. Sel. Topics Quantum Electron.*, vol. 26, no. 5, pp. 1–8, Sep. 2020.

[19] K. Maru, K. Tanaka, T. Chiba, H. Nonen, and H. Uetsuka, "Dynamic gain equalizer using proposed adjustment procedure for thermooptic phase shifters under the influence of thermal crosstalk," *J. Lightw. Technol.*, vol. 22, no. 6, pp. 1523–1532, Jun. 2004.

[20] M. Milanizadeh, D. Aguiar, F. Morichetti, and A. Melloni, "Automatic configuration and wavelength locking of coupled micro-ring resonators in presence of thermal cross-talk," in *Proc. 20th Int. Conf. Transparent Opt. Netw. (ICTON)*, Jul. 2018, pp. 1–4.

[21] M. Milanizadeh, D. Aguiar, A. Melloni, and F. Morichetti, "Canceling thermal cross-talk effects in photonic integrated circuits," *J. Lightw. Technol.*, vol. 37, no. 4, pp. 1325–1332, Feb. 15, 2019, doi: 10.1109/JLT.2019.2892512.

[22] C. T. DeRose, N. J. Martinez, R. D. Kekatpure, W. A. Zortman, A. L. Starbuck, A. Pomerene, and A. L. Lentine, "Thermal crosstalk limits for silicon photonic DWDM interconnects," in *Proc. Opt. Interconnects Conf.*, San Diego, CA, USA, May 2014, pp. 125–126, doi: 10.1109/OIC.2014.6886111.

[23] M. Jacques, A. Samani, E. El-Fiky, D. Patel, Z. Xing, and D. V. Plant, "Optimization of thermo-optic phase-shifter design and mitigation of thermal crosstalk on the SOI platform," *Opt. Express*, vol. 27, no. 8, pp. 10456–10471, 2019.

[24] C. Qiu, Y. Wang, Y. Chen, Y. Lei, L. Qin, and L. Wang, "Design and analysis of a novel graphene-assisted silica/polymer hybrid waveguide with thermal–optical phase modulation structure," *IEEE Photon. J.*, vol. 11, no. 2, Apr. 2019, Art. no. 4900410.

[25] S. Zhu, T. Hu, Z. Xu, Y. Dong, Q. Zhong, Y. Li, and N. Singh, "An improved thermo-optic phase shifter with AlN block for silicon photonics," in *Proc. Opt. Fiber Commun. Conf. (OFC)*, San Diego, CA, USA, 2019, pp. 1–3.

[26] P. Pintus, M. Hofbauer, and C. L. Manganelli, "PWM-driven thermally tunable silicon microring resonators: Design, fabrication, and characterization," *Laser Photon. Rev.*, vol. 13, no. 9, Sep. 2019, Art. no. 1800275.

[27] M. R. Watts, W. A. Zortman, D. C. Trotter, G. N. Nielson, D. L. Luck, and R. W. Young, "Adiabatic resonant microrings (ARMs) with directly integrated thermal microphotonics," in *Proc. Conf. Lasers Electro-Opt./Int. Quantum Electron. Conf.*, Baltimore, MD, USA, 2009, pp. 1–2, doi: 10.1364/CLEO.2009.CPDB10.

[28] A. Masood, M. Pantouvaki, G. Lepage, P. Verheyen, J. Van Campenhout, P. Absil, D. Van Thourhout, and W. Bogaerts, "Comparison of heater architectures for thermal control of silicon photonic circuits," in *Proc. 10th Int. Conf. Group IV Photon.*, Aug. 2013, pp. 83–84, doi: 10.1109/Group4.2013.6644437.

[29] Lumerical. *MODE: Waveguide Simulator, HEAT: 3D Heat Transport Simulator, CHARGE: 3D Charge Transport Simulator, INTERCONNECT: Photonic Integrated Circuit Simulator*. [Online]. Available: https://www.lumerical.com/products/

[30] D. Mishra and R. K. Sonkar, "Design and analysis of a graded-index strained Si_{1-x} Ge_x optical PN phase shifter," *IEEE Photon. J.*, vol. 10, no. 6, Dec. 2018, Art. no. 6101214.

[31] Z. Chu, Y. Liu, J. Sheng, L. Wang, J. Du, and K. Xu, "On-chip optical attenuators designed by artifical neural networks," in *Proc. Asia Commun. Photon. Conf. (ACP)*, Hangzhou, China, Oct. 2018, pp. 1–3.

[32] S. M. Sze and K. N. Kwok, *Physics of Semiconductor Devices*. Hoboken, NJ, USA: Wiley, 2006.

SOUVARAJ DE (Student Member, IEEE) received the B.Tech. degree in electronics and communication engineering from the National Institute of Technology, Calicut, India, in 2016, and the M.Tech. degree in optoelectronics and optical communication from IIT Delhi, India in 2020.

He has been working as a Visiting Researcher with the THz Photonics Group, Technische Universität Braunschweig, Germany, since 2019. He is currently working as a Scientist with Physikalisch-Technische Bundesanstalt (PTB), Braunschweig, Germany. His current research interests include silicon photonics, high-frequency communication, and THz photonics for 6G and beyond. He was a recipient of the DAAD Fellowship.

RANJAN DAS (Member, IEEE) received the B.E. degree in electronics and instrumentation engineering from Jadavpur University, India, and the master's and Ph.D. degrees from the Electrical Engineering Department, IIT Bombay, Mumbai, India, in 2018. He was with the Electronics and Electrical Engineering Department, South University of Science and Technology of China, Shenzhen, China, as a Visiting Researcher. He is currently a Postdoctoral Researcher with Technische Universität Braunschweig, Germany. His major research interests include THz photonics for wireless communication, photonic signal processing, integrated photonics, reconfigurable microwave components designs, and real-time analog signal processing.

RAVI K. VARSHNEY is currently working as a Professor of physics with IIT Delhi. He has been a Visiting Scientist at various universities such as the University of Florida, USA, the University of Strathclyde, U.K., the University of Twente, The Netherlands, and the University of Nice Sophia Antipolis, France. His current research interests include silicon photonics, specialty fibers, and THz photonics. Dr. Varshney is a Fellow of OSI and a member of the OSA. He was a recipient of the Fulbright and Marie Curie Fellowships.

THOMAS SCHNEIDER received the Diploma degree in electrical engineering from Humboldt Universität zu Berlin, Berlin, Germany, in 1995, and the Ph.D. degree in physics from the Brandenburgische Technische Universität Cottbus, Cottbus, Germany, in 2000. From 2000 to 2013, he was with the Deutsche Telekom Hochschule für Telekommunikation (HfT), Leipzig, Germany. From 2006 to 2013, he was the Head of HfT. Since 2014, he has been the Head of the Terahertz-Photonics Group, Institut für Hochfrequenztechnik, Technische Universität Braunschweig, Braunschweig, Germany. His current research interests include nonlinear optical effects in telecommunication systems and sensors, slow and fast light, high-resolution spectroscopy, the generation of millimeter and THz waves, optical sampling, and integrated photonics.